

# Toxicity Profiling of Engineered Nanomaterials via Multivariate Dose Response Surface Modeling

TRINA PATEL<sup>1</sup>, DONATELLO TELESCA<sup>1</sup>,  
SAJI GEORGE<sup>2,3</sup>, ANDRÉ E. NEL<sup>2,3</sup>

Author's Footnote

<sup>1</sup> UCLA School of Public Health, Department of Biostatistics.

<sup>2</sup> UCLA Department of Medicine, Division of NanoMedicine.

<sup>3</sup> UCLA California NanoSystems Institute.

December 12, 2011

## SUPPLEMENTARY MATERIALS

### APPENDIX A: FULL CONDITIONAL DISTRIBUTIONS

In this appendix we describe some of the full conditional distributions for the model described in the paper. Let  $y_{ijk}(d, t)$  denote a multivariate response corresponding to ENM  $i$  ( $i = 1, \dots, I$ ), cytotoxicity parameter  $j$  ( $j = 1, \dots, J$ ), and replicate  $k$  ( $k = 1, \dots, K$ ) at some dose  $d$  in  $d = (d_1, \dots, d_D)'$  and some time  $t$  in  $t = (t_1, \dots, t_T)'$ .

Also, let  $\boldsymbol{\theta} = (\boldsymbol{\alpha}, \boldsymbol{\beta}, \boldsymbol{\gamma}, \boldsymbol{\phi}, \boldsymbol{\psi}, \boldsymbol{\alpha}_o, \boldsymbol{\beta}_o, \boldsymbol{\gamma}_o, \boldsymbol{\tau}, \boldsymbol{\sigma}_\epsilon, \boldsymbol{\sigma}_\alpha, \boldsymbol{\sigma}_\beta, \boldsymbol{\sigma}_\gamma)$  denote the full parameter vector and, let  $\boldsymbol{\theta}_{\setminus \delta}$  denote the vector containing all components of  $\boldsymbol{\theta}$  except for some parameter  $\delta$  in  $\boldsymbol{\theta}$ . Moreover, we denote  $\mathbf{Y}_{ij}$  as the complete set of response values for particle  $i$  and outcome  $j$ . Using the notation above we define the full conditional distributions for all available parameters as follows.

A.1: Full conditional distributions for the random effect parameters  $\alpha_{ij}$ ,  $\beta_{ij}$ ,  $\gamma_{ij}$ , and  $\delta_{ij}$

$$\alpha_{ij} \mid \mathbf{Y}_{ij}, \boldsymbol{\theta}_{\setminus \alpha_{ij}} \sim N \left( \frac{\frac{\sum_{d,t,k} \tilde{y}_{\alpha_{ijk}}(d,t)}{\sigma_{\epsilon_j}^2 / \tau_i} + \frac{\alpha_{oi}}{\sigma_{\alpha_i}}}{\frac{D \times T \times K}{\sigma_{\epsilon_j}^2 / \tau_i} + \frac{1}{\sigma_{\alpha_i}}} , \frac{1}{\frac{D \times T \times K}{\sigma_{\epsilon_j}^2 / \tau_i} + \frac{1}{\sigma_{\alpha_i}}} \right)$$

where,

$$\tilde{y}_{\alpha_{ijk}}(d, t) = \begin{cases} y_{ijk}(d, t) - \mathcal{B}(d, \phi_{ij})' \beta_{ij} - \mathcal{B}(t, \psi_{ij})' \gamma_{ij} & \text{if } \rho_{ij} = 0 \\ y_{ijk}(d, t) - \mathcal{B}(d, \phi_{ij})' \beta_{ij} - \mathcal{B}(t, \psi_{ij})' \gamma_{ij} - \mathcal{B}(d * t, \chi_{ij})' \delta_{ij} & \text{if } \rho_{ij} = 1 \end{cases}$$

$\beta_{ij} \mid \mathbf{Y}_{ij}, \boldsymbol{\theta}_{\setminus \beta_{ij}} \sim N_4$

$$\left( \left( \Sigma_{\beta_i}^{-1} + \sum_{d,t,k} \frac{\mathcal{B}(d, \phi_{ij}) \mathcal{B}(d, \phi_{ij})'}{\sigma_{\epsilon_j}^2 / \tau_i} \right)^{-1} \left( \Sigma_{\beta_i}^{-1} \beta_{oi} + \sum_{d,t,k} \frac{\mathcal{B}(d, \phi_{ij}) \tilde{y}_{\beta_{ijk}}(d,t)}{\sigma_{\epsilon_j}^2 / \tau_i} \right), \left( \Sigma_{\beta_i}^{-1} + \sum_{d,t,k} \frac{\mathcal{B}(d, \phi_{ij}) \mathcal{B}(d, \phi_{ij})'}{\sigma_{\epsilon_j}^2 / \tau_i} \right)^{-1} \right)$$

where,

$$\tilde{y}_{\beta_{ijk}}(d, t) = \begin{cases} y_{ijk}(d, t) - \mathcal{B}(t, \psi_{ij})' \gamma_{ij} - \alpha_{ij} & \text{if } \rho_{ij} = 0 \\ y_{ijk}(d, t) - \mathcal{B}(t, \psi_{ij})' \gamma_{ij} - \mathcal{B}(d * t, \chi_{ij})' \delta_{ij} - \alpha_{ij} & \text{if } \rho_{ij} = 1 \end{cases}$$

$\gamma_{ij} \mid \mathbf{Y}_{ij}, \boldsymbol{\theta}_{\setminus \gamma_{ij}} \sim N_4$

$$\left( \left( \Sigma_{\gamma_i}^{-1} + \sum_{d,t,k} \frac{\mathcal{B}(t, \psi_{ij}) \mathcal{B}(t, \psi_{ij})'}{\sigma_{\epsilon_j}^2 / \tau_i} \right)^{-1} \left( \Sigma_{\gamma_i}^{-1} \gamma_{oi} + \sum_{d,t,k} \frac{\mathcal{B}(t, \psi_{ij}) \tilde{y}_{\gamma_{ijk}}(d,t)}{\sigma_{\epsilon_j}^2 / \tau_i} \right), \left( \Sigma_{\gamma_i}^{-1} + \sum_{d,t,k} \frac{\mathcal{B}(t, \psi_{ij}) \mathcal{B}(t, \psi_{ij})'}{\sigma_{\epsilon_j}^2 / \tau_i} \right)^{-1} \right)$$

where,

$$\tilde{y}_{\gamma_{ijk}}(d, t) = \begin{cases} y_{ijk}(d, t) - \mathcal{B}(d, \phi_{ij})' \beta_{ij} - \alpha_{ij} & \text{if } \rho_{ij} = 0 \\ y_{ijk}(d, t) - \mathcal{B}(d, \phi_{ij})' \beta_{ij} - \mathcal{B}(d * t, \chi_{ij})' \delta_{ij} - \alpha_{ij} & \text{if } \rho_{ij} = 1 \end{cases}$$

$\delta_{ij} \mid \mathbf{Y}_{ij}, \boldsymbol{\theta}_{\setminus \delta_{ij}} \sim N_4$

$$\left( \left( \Sigma_{\delta_i}^{-1} + \sum_{d,t,k} \frac{\mathcal{B}(t, \chi_{ij}) \mathcal{B}(d * t, \chi_{ij})'}{\sigma_{\epsilon_j}^2 / \tau_i} \right)^{-1} \left( \Sigma_{\delta_i}^{-1} \mathbf{m}_{\delta_{ij}} + \sum_{d,t,k} \frac{\mathcal{B}(d * t, \chi_{ij}) \tilde{y}_{\delta_{ijk}}(d,t)}{\sigma_{\epsilon_j}^2 / \tau_i} \right), \left( \Sigma_{\gamma_i}^{-1} + \sum_{d,t,k} \frac{\mathcal{B}(t, \psi_{ij}) \mathcal{B}(t, \psi_{ij})'}{\sigma_{\epsilon_j}^2 / \tau_i} \right)^{-1} \right)$$

where,  $\tilde{y}_{\delta_{ijk}}(d, t) = y_{ijk}(d, t) - \mathcal{B}(d, \phi_{ij})' \beta_{ij} - \mathcal{B}(t, \psi_{ij})' \gamma_{ij} - \alpha_{ij}$

A.2: Full conditional distributions for ENM level parameters  $\alpha_{oi}$ ,  $\beta_{oi}$ , and  $\gamma_{oi}$

$$\alpha_{oi} \mid \boldsymbol{\theta}_{\setminus \alpha_{ij}} \sim N \left( \frac{\frac{\sum_{j=1}^J \alpha_{ij}}{\sigma_{\alpha_i}^2} + \frac{m_{\alpha_i}}{s_{\alpha_i}^2}}{\frac{J}{\sigma_{\alpha_i}^2} + \frac{1}{s_{\alpha_i}^2}}, \frac{1}{\frac{J}{\sigma_{\alpha_i}^2} + \frac{1}{s_{\alpha_i}^2}} \right)$$

$$\beta_{oi} \mid \boldsymbol{\theta}_{\setminus \beta_{ij}} \sim N_4 \left( (J\Sigma_{\beta_i}^{-1} + \mathbf{v}_{\beta_i}^{-1})^{-1} \left( \Sigma_{\beta_i}^{-1} \sum_{j=1}^J \beta_{ij} + \mathbf{v}_{\beta_i}^{-1} \mathbf{m}_{\beta_i} \right), (J\Sigma_{\beta_i}^{-1} + \mathbf{v}_{\beta_i}^{-1})^{-1} \right)$$

$$\gamma_{oi} \mid \boldsymbol{\theta}_{\setminus \gamma_{ij}} \sim N_4 \left( (J\Sigma_{\gamma_i}^{-1} + \mathbf{v}_{\gamma_i}^{-1})^{-1} \left( \Sigma_{\gamma_i}^{-1} \sum_{j=1}^J \gamma_{ij} + \mathbf{v}_{\gamma_i}^{-1} \mathbf{m}_{\gamma_i} \right), (J\Sigma_{\gamma_i}^{-1} + \mathbf{v}_{\gamma_i}^{-1})^{-1} \right)$$

A.3: Full conditional distributions for the error variance parameter  $\sigma_{\epsilon_j}^2$  and variance inflation parameter  $\tau_i$

$$1/\sigma_{\epsilon_j}^2 \mid \mathbf{Y}_{ij}, \boldsymbol{\theta}_{\setminus \sigma_{\epsilon_j}} \sim \text{Gamma} \left( a_{\epsilon_j} + \frac{I \times D \times T \times K}{2}, \frac{1}{2} \sum_{d,t,k,i} (y_{ijk}(d,t) - m_{ij}(d,t))^2 \tau_i + b_{\epsilon_j} \right)$$

where,

$$m_{ij}(d,t) = \begin{cases} \mathcal{B}(d, \phi_{ij})' \boldsymbol{\beta}_{ij} + \mathcal{B}(t, \psi_{ij})' \boldsymbol{\gamma}_{ij} + \alpha_{ij} & \text{if } \rho_{ij} = 0 \\ \mathcal{B}(d, \phi_{ij})' \boldsymbol{\beta}_{ij} + \mathcal{B}(t, \psi_{ij})' \boldsymbol{\gamma}_{ij} + \mathcal{B}(d * t, \chi_{ij})' \boldsymbol{\gamma}_{ij} + \alpha_{ij} & \text{if } \rho_{ij} = 1 \end{cases}$$

$$\tau_i \mid \mathbf{Y}_{ij}, \boldsymbol{\theta}_{\setminus \tau_i} \sim \text{Gamma} \left( \frac{\nu}{2} + \frac{J \times K \times D \times T}{2}, \frac{1}{2} \sum_{d,t,k,j} \frac{(y_{ijk}(d,t) - m_{ij}(d,t))^2}{\sigma_{\epsilon_j}^2} + \frac{\nu}{2} \right)$$

where,

$$m_{ij}(d,t) = \begin{cases} \mathcal{B}(d, \phi_{ij})' \boldsymbol{\beta}_{ij} + \mathcal{B}(t, \psi_{ij})' \boldsymbol{\gamma}_{ij} + \alpha_{ij} & \text{if } \rho_{ij} = 0 \\ \mathcal{B}(d, \phi_{ij})' \boldsymbol{\beta}_{ij} + \mathcal{B}(t, \psi_{ij})' \boldsymbol{\gamma}_{ij} + \mathcal{B}(d * t, \chi_{ij})' \boldsymbol{\gamma}_{ij} + \alpha_{ij} & \text{if } \rho_{ij} = 1 \end{cases}$$

A.4: Full conditional distributions for other variance parameters

$$1/\sigma_{\alpha_i}^2 \mid \boldsymbol{\theta}_{\setminus \sigma_{\alpha_i}} \sim \text{Gamma} \left( a_{\alpha_i} + \frac{J}{2}, \frac{1}{2} \sum_{j=1}^J (\alpha_{ij} - \alpha_{oi})^2 + b_{\alpha_i} \right)$$

$$1/\sigma_{\beta_{i\ell}}^2 \mid \boldsymbol{\theta}_{\setminus \sigma_{\beta_{i\ell}}} \sim \text{Gamma} \left( a_{\beta_i} + \frac{J}{2}, \frac{1}{2} \sum_{j=1}^J (\beta_{ij\ell} - \beta_{oi\ell})^2 + b_{\beta_i} \right)$$

$$1/\sigma_{\gamma_{i\ell}}^2 \mid \boldsymbol{\theta}_{\setminus \sigma_{\gamma_{i\ell}}} \sim \text{Gamma} \left( a_{\gamma_i} + \frac{J}{2}, \frac{1}{2} \sum_{j=1}^J (\gamma_{ij\ell} - \gamma_{oi\ell})^2 + b_{\gamma_i} \right)$$

where,  $\ell = 1, \dots, 4$

## APPENDIX B: SIMULATION STUDY

To assess estimation of the model presented in the paper, we simulated four sets ( $i = 1, \dots, 4$ ) of four independent surfaces ( $j = 1, \dots, 4$ ), each evaluated at ten doses ( $d \in [0, D]$ ) and seven times of exposure ( $t \in [0, T]$ ). The dose and time kinetics were simulated in an additive fashion from various parametric functions. In addition, for each set of response surfaces we simulated a dose\*time interaction function for two of the four surfaces. If we let  $y_{ijk}(d, t)$  denote a multivariate response corresponding to a set of surfaces  $i$  ( $i = 1, \dots, 4$ ), outcome  $j$  ( $j = 1, \dots, 4$ ), and replicate  $k$  ( $k = 1, \dots, 4$ ) at dose  $d \in [0, D]$  and time  $t \in [0, T]$  then each simulated surface can be described by

$$y_{ijk}(d, t) = s_{ij}(d, t) + \xi_{ijk}(d, t). \quad (1)$$

where  $s_{ij}(d, t) = \alpha_{ij} + r_{ij}(d) + u_{ij}(t) + w_{ij}(dt)I(r_{ij} = 1)$  represents a smooth dose-response surface and  $r_{ij}$  is an indicator which determines whether or not a dose-time interaction was simulated. The functions  $r_{ij}(d)$ ,  $u_{ij}(t)$  and  $w_{ij}(dt)$ , were simulated from various parametric functions such as log-logistic, weibull, polynomials, and cubic splines. These parametric functions were used to construct both canonical and non-canonical profiles that are still reasonably interpretable in a toxicity framework. Note that the simulated response curves do not follow our model which uses a B-spline representation with two random interior knots. Dose-response surfaces were also simulated with varying levels of noise across each outcome  $j$ . This is as expected in high throughput screening studies where different assay systems are able to capture measurements with varying levels of precision. More specifically,  $\xi_{ijk}(d, t) \sim N(0, \sigma_{\xi_j})$ , where  $\sigma_{\xi_j} = .6, .8, 1, 1.2$  for  $j = 1, \dots, 4$  respectively.

The model described in the paper was fit to the simulated surfaces. We placed relatively diffuse priors on all parameters. More precisely, we placed  $Gamma(.01, .01)$  priors on the  $1/\sigma_{\epsilon_j}$  parameters,  $Gamma(1, .1)$  priors on all remaining precision parameters, and a prior

that is uniform on 1,2,4,8,16, and 32, for our degrees of freedom parameter  $\nu$ . The population level parameters  $\alpha_{o_i}$  are modeled as  $N(0, 10)$  and the  $\beta_{o_i}$  and  $\gamma_{o_i}$  parameters as truncated  $N_4(\mathbf{0}, 10\mathbf{I})$ . We also fixed  $\beta_{ij2} = 0$ ,  $\gamma_{ij2} = 0$  and  $\delta_{ij2} = 0$  assuming no effect before the first change-points. Note that this constraint can be changed to  $\beta_{ij2} \leq 0$ ,  $\gamma_{ij2} \leq 0$  and  $\delta_{ij2} \leq 0$ , when assuming a tonic effect before the first change-point. We placed a diffuse  $N_4(\mathbf{0}, 100\mathbf{I})$  prior on our dose-time interaction amplitude parameters  $\delta_{ij}$ . Finally, in order to assess the sensitivity of the model results to our choice of prior parameters, we specified increasingly informative priors on our population level change-point parameters  $\lambda_{\phi_i}$  and  $\lambda_{\psi_i}$ , and our dose-time interaction change-point parameters  $\chi_{ij}$ . Our inferences are based on 20,000 MCMC samples after discarding a conservative 60,000 iterations for burn-in.

Figure 1 gives examples of increasingly informative prior distributions on our dose-response change-point parameters  $\phi_{ij1}$  and  $\phi_{ij2}$ . We impose a right-skewed prior distribution on  $\phi_{ij1}$ , which favors (a-priori) conservative values for the location of the first change-point parameter, and allow a relatively diffuse prior distribution for our second change-point parameter  $\phi_{ij2}$ . Similar examples can be constructed for our duration response change-points  $\psi_{ij1}$  and  $\psi_{ij2}$  and our dose-time interaction change-points  $\chi_{ij1}$  and  $\chi_{ij2}$ .

Figures 2 through 5 provide results from our simulation study using increasingly informative priors on our population level change-point parameters  $\lambda_{\phi_i}$  and  $\lambda_{\psi_i}$  and our dose-time interaction change-point parameters  $\chi_{ij}$ . Simulated dose (*column 2*), duration (*column 3*), and dose-time interaction (*column 4*) response curves are superimposed with expected dose and duration response curves and point-wise 95% posterior intervals estimated from our model. Prior 1 (blue) is the least informative and corresponds to a set of relatively diffuse  $Gamma(2, 1)$  and  $Gamma(3, 1)$  priors on  $\lambda_{\phi_i}$  and  $\lambda_{\psi_i}$ , and a diffuse  $B_2(2, 3, 1, 1, DT)$  prior on  $\chi_{ij}$ . Prior 2 is moderately informative  $Gamma(2.5, 1)$  and  $Gamma(7, 1.5)$  prior on  $\lambda_{\phi_i}$  and  $\lambda_{\psi_i}$ , and a  $B_2(2.5, 4.7, 1, 1, DT)$  prior on  $\chi_{ij}$ . Finally, prior 3 is the most informa-

tive and corresponds to a  $\text{Gamma}(2, 1)$  and  $\text{Gamma}(7, 1.5)$  prior on  $\boldsymbol{\lambda}_{\phi_i}$  and  $\boldsymbol{\lambda}_{\phi_i}$ , and a  $B_2(2, 4.7, 1, 1, DT)$  prior on  $\boldsymbol{\chi}_{ij}$ . The *left panel* shows fitted dose-response surfaces, spanning dose and time, for our least informative prior. Table 1 also provides posterior mean estimates of  $\rho_{ij}$ , which is the expected inclusion probability of the dose-time interaction function, after adjusting for multiplicity, and can be used to test for a dose-time interaction.

These figures show that the posterior mean response trajectories are able to adequately estimate the true dose and duration response curves while capturing the most important features. In particular, our model is able to appropriately model both canonical and non-canonical dose-response trajectories while providing interpretable risk assessment parameters. It is also evident that our model is relatively insensitive to the choice of prior parameters for our change-points. Priors 1-3 are, in most cases, indistinguishable, especially in those cases where the data sufficiently provide information on the location of the change-points. Finally, although we do not include a formal simulation study to determine the false positive and negative rate for correctly identifying an interaction function using our model, we do notice that in all the simulated cases the model is able to correctly distinguish between data simulated with and without a dose\*time interaction function.

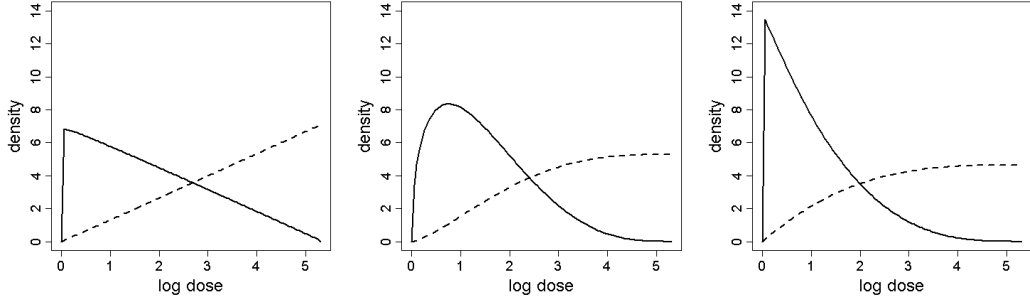


Figure 1: **Marginal prior distributions on the change-points parameters.** Examples of increasingly informative prior distributions on the change-point parameters  $\phi_{ij1}$ ,  $\phi_{ij2}$ . We favor (a-priori) the choice of conservative values for the location of the first change-point (*solid line*) and a relatively diffuse prior for our second change-point (*dotted line*).

Prior	ENM	Outcome 1	Outcome 2	Outcome 3	Outcome 4
Prior1	1	0.01	0.99	0.99	0.00
	2	0.00	0.00	0.99	0.99
	3	0.99	0.00	0.99	0.00
	4	0.99	0.99	0.01	0.00
Prior2	1	0.00	0.98	0.99	0.00
	2	0.00	0.00	0.99	0.99
	3	0.99	0.00	0.99	0.00
	4	0.99	0.99	0.00	0.00
Prior3	1	0.00	0.99	0.99	0.00
	2	0.00	0.01	0.99	0.99
	3	0.99	0.00	0.99	0.11
	4	0.99	0.99	0.00	0.00

Table 1: **Expected inclusion probability of the dose-time interaction function using priors 1-3.** Posterior mean estimates of  $\rho_{ij}$  describe the expected inclusion probability of the dose-time interaction function and can be used to test for an interaction.

## APPENDIX C: SIMULATION STUDY 2

To assess sensitivity of our model to our choice of a prior model on our change-point parameters, we conducted a sensitivity analysis using the simulated data described above. We fit the

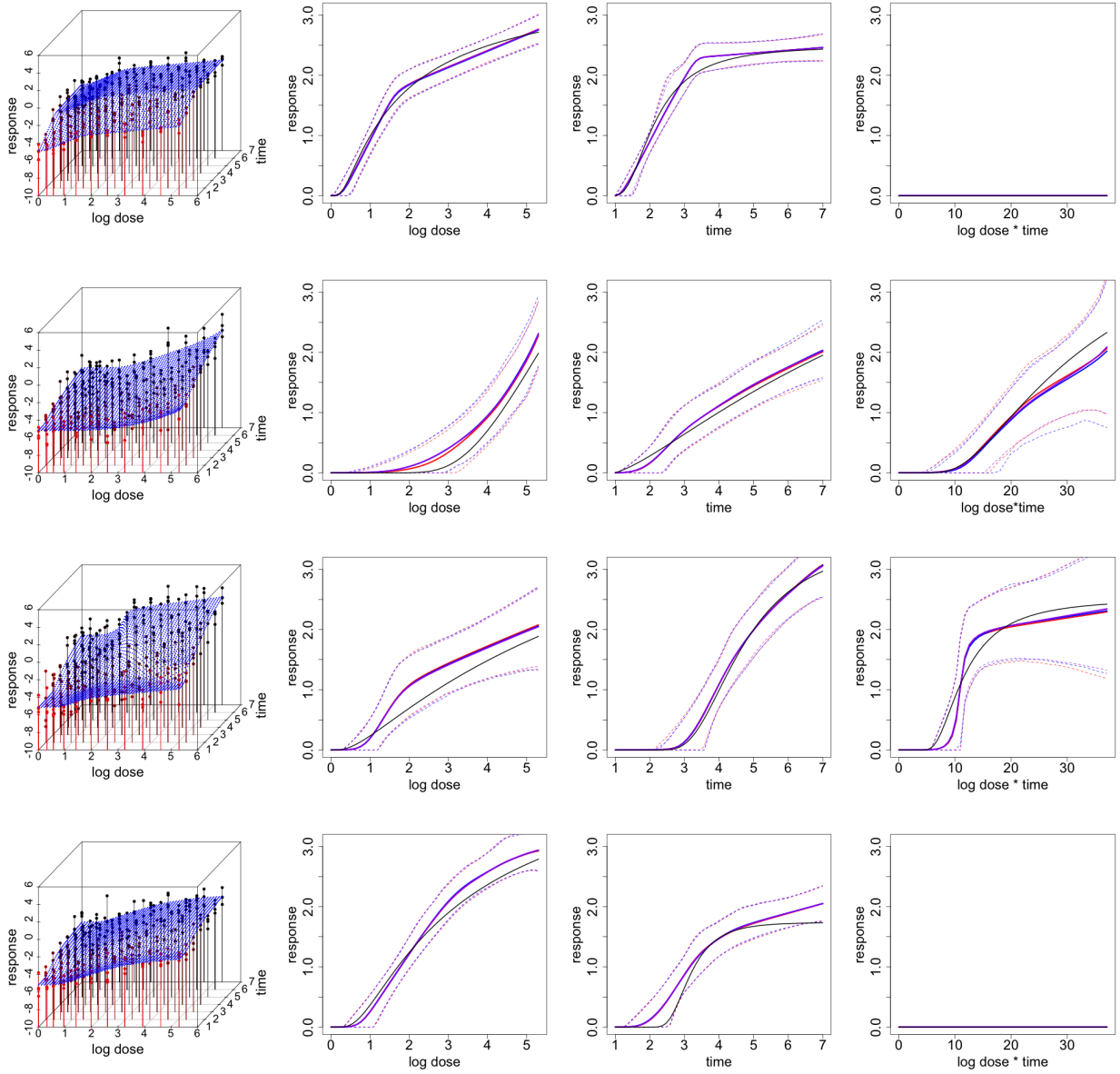


**Figure 2: Simulation study to assess model fit and prior sensitivity.** Simulated dose (*column 2*), duration (*column 3*), and dose-time interaction (*column 4*) response curves (black) superimposed with expected curves estimated from our model (solid colored lines) and point-wise 95% posterior intervals (dashed lines). Prior 1 (blue) is the least informative, prior 2 (red) is moderately informative and priors 3 (purple) is the most informative. (*column 1*) Fitted response surfaces estimated using prior 1, superimposed with simulated data.

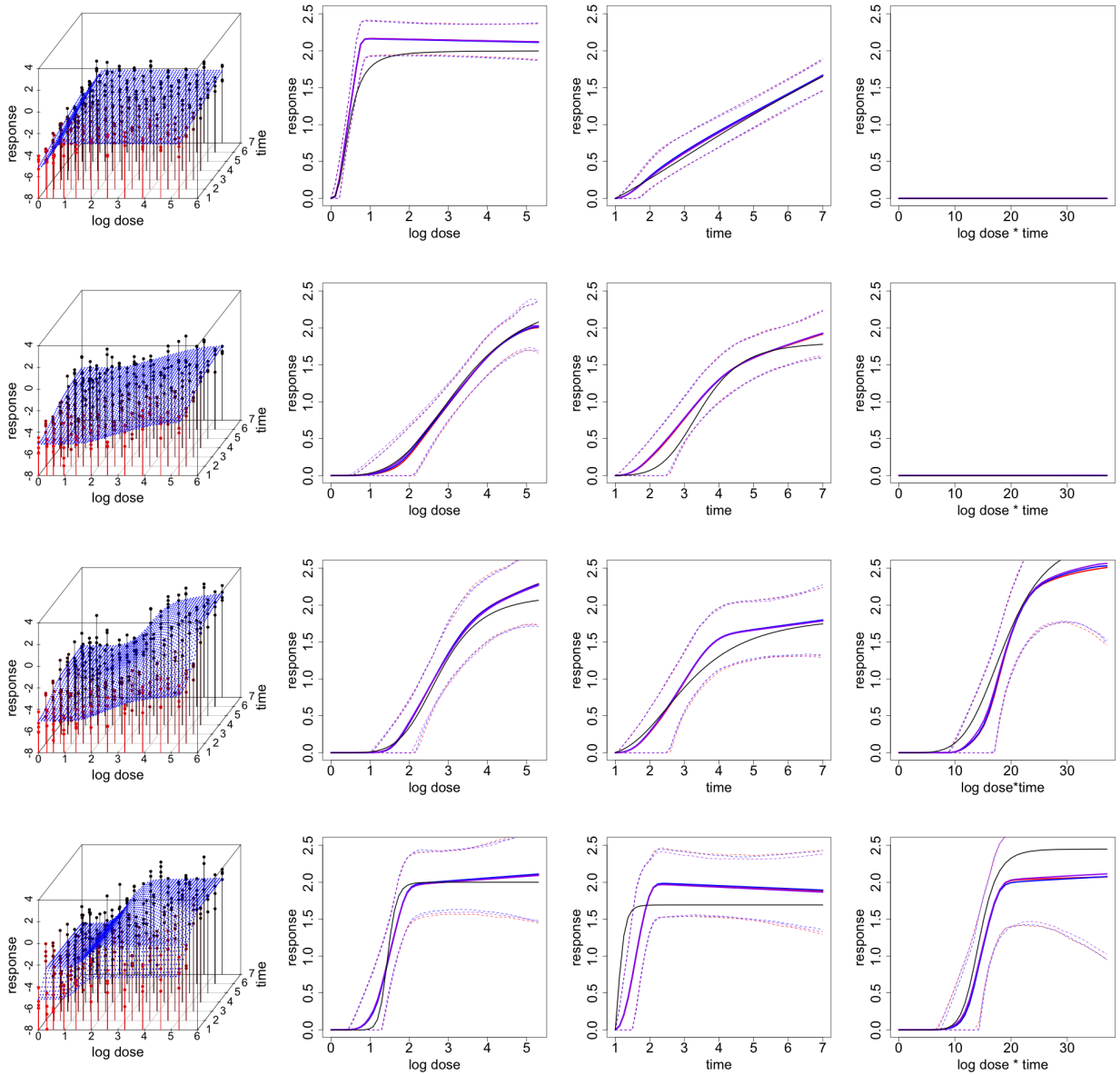


**Figure 3: Simulation study to assess model fit and prior sensitivity.** Simulated dose (*column 2*), duration (*column 3*), and dose-time interaction (*column 4*) response curves (black) superimposed with expected curves estimated from our model (solid colored lines) and point-wise 95% posterior intervals (dashed lines). Prior 1 (blue) is the least informative, prior 2 (red) is moderately informative and priors 3 (purple) is the most informative. (*column 1*) Fitted response surfaces estimated using prior 1, superimposed with simulated data.

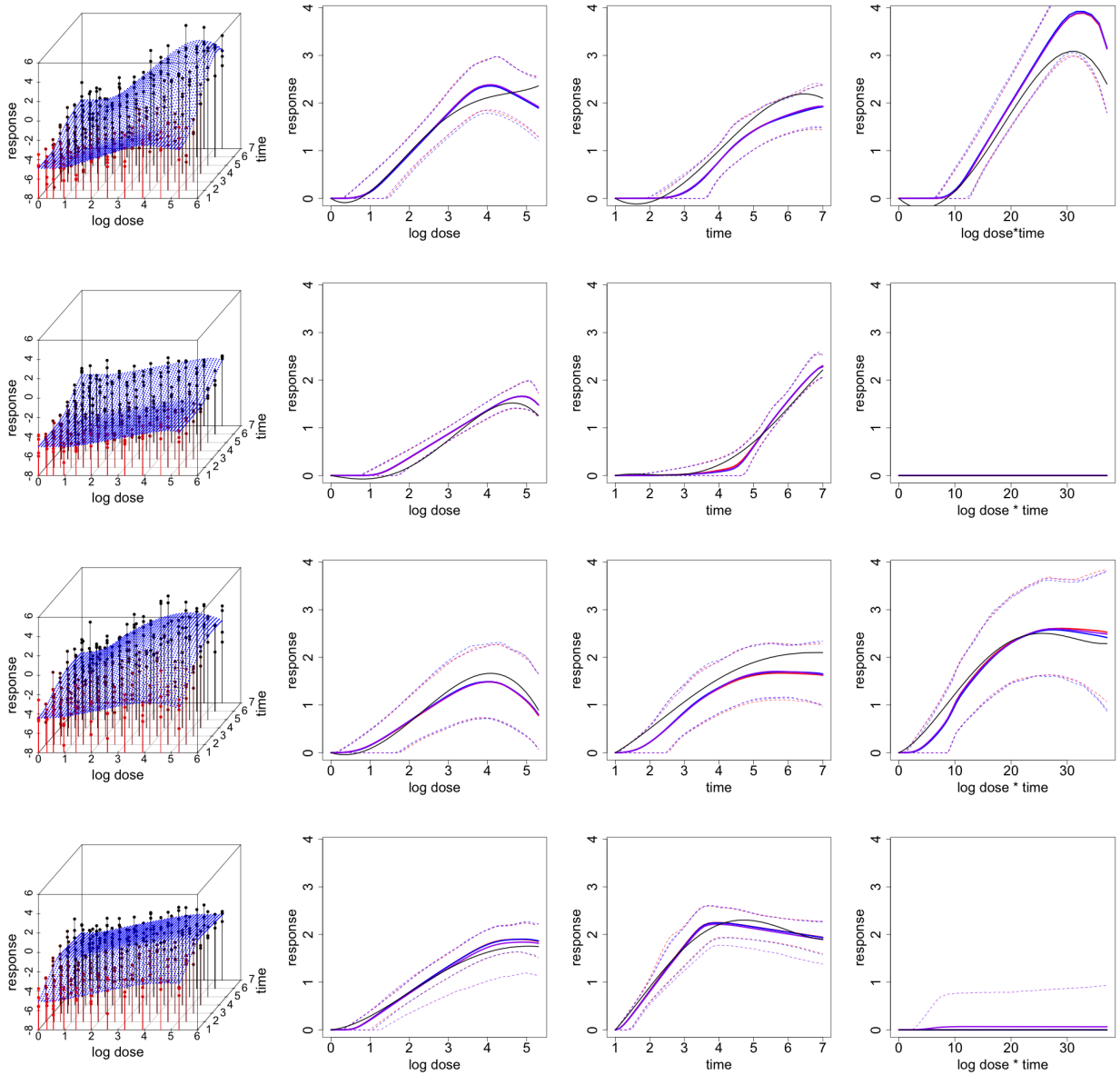


**Figure 4: Simulation study to assess model fit and prior sensitivity.** Simulated dose (*column 2*), duration (*column 3*), and dose-time interaction (*column 4*) response curves (black) superimposed with expected curves estimated from our model (solid colored lines) and point-wise 95% posterior intervals (dashed lines). Prior 1 (blue) is the least informative, prior 2 (red) is moderately informative and priors 3 (purple) is the most informative. (*column 1*) Fitted response surfaces estimated using prior 1, superimposed with simulated data.

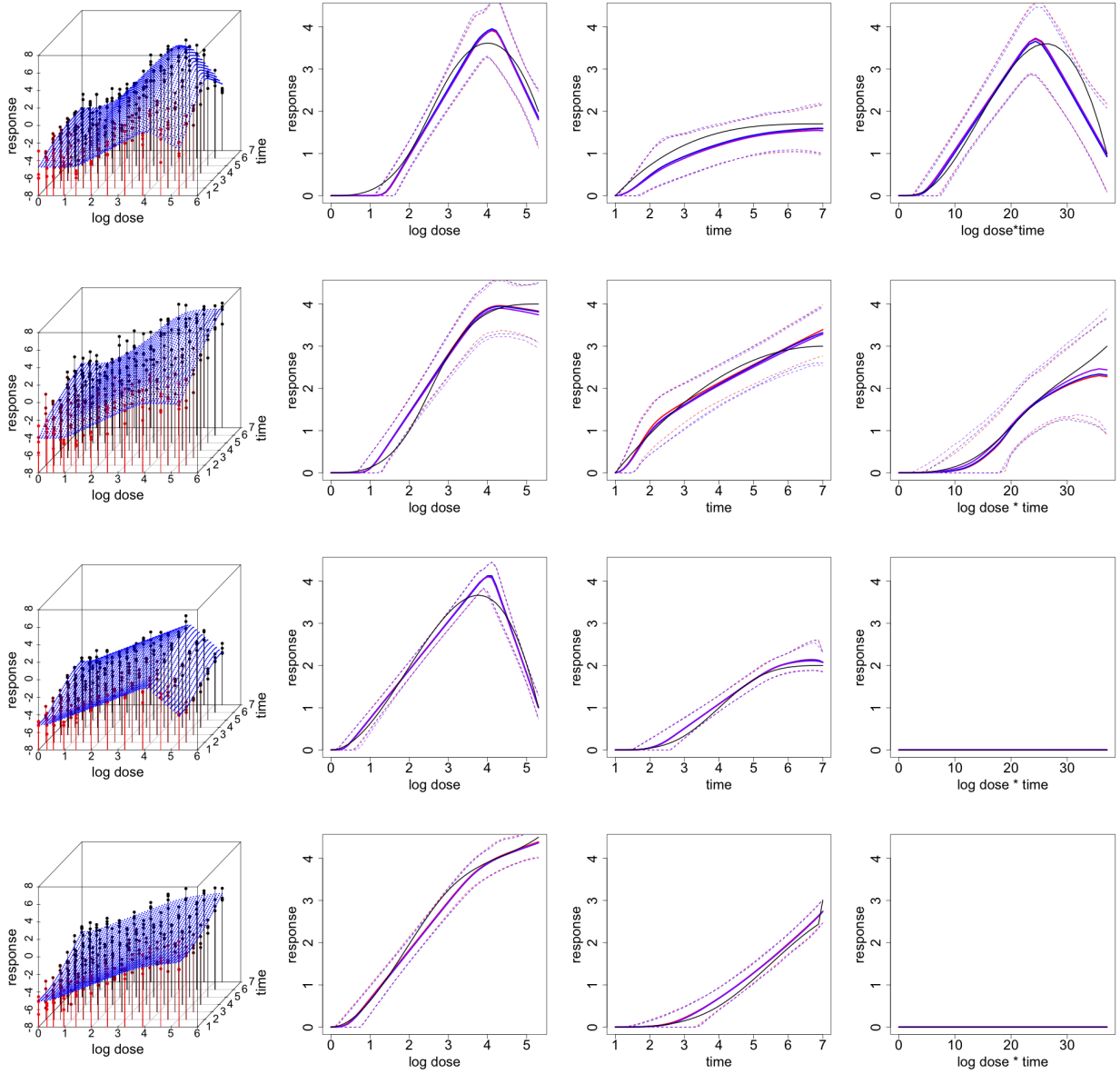


**Figure 5: Simulation study to assess model fit and prior sensitivity.** Simulated dose (*column 2*), duration (*column 3*), and dose-time interaction (*column 4*) response curves (black) superimposed with expected curves estimated from our model (solid colored lines) and point-wise 95% posterior intervals (dashed lines). Prior 1 (blue) is the least informative, prior 2 (red) is moderately informative and priors 3 (purple) is the most informative. (*column 1*) Fitted response surfaces estimated using prior 1, superimposed with simulated data.

simulated data to models with three different priors on our change-point parameters. The first prior was the bivariate beta prior parameterization described above, where we impose a right-skewed prior distribution on  $\phi_{ij1}$ ,  $\psi_{ij1}$  and  $\chi_{ij1}$ , and allow a conditionally uniform prior distribution for our second change-point parameters  $\phi_{ij2}$ ,  $\psi_{ij2}$  and  $\chi_{ij2}$ . Here we specified a set of relatively diffuse  $Gamma(2, 1)$  and  $Gamma(3, 1)$  priors for our population level change-point parameters  $\boldsymbol{\lambda}_{\phi_i}$  and  $\boldsymbol{\lambda}_{\phi_i}$ , and a diffuse  $B_2(2, 3, 1, 1, DT)$  prior for our dose-time interaction change-point parameter  $\boldsymbol{\chi}_{ij}$ . The second prior is another parameterization of the bivariate beta distribution which allows for a uniform prior on the simlex, and can be described as follows:

$$\begin{aligned}\boldsymbol{\phi}_{ij} &\sim B_2(1, 1, 1, 1, D), \\ \boldsymbol{\psi}_{ij} &\sim B_2(1, 1, 1, 1, T), \\ \boldsymbol{\chi}_{ij} &\sim B_2(1, 1, 1, 1, T).\end{aligned}\tag{2}$$

with support  $\mathcal{S}(\boldsymbol{\phi}_{ij}) = \{(\phi_{ij1}, \phi_{ij2}) : 0 < \phi_{ij1} < \phi_{ij2} < D\}$  and  $\mathcal{S}(\boldsymbol{\psi}_{ij}) = \{(\psi_{ij1}, \psi_{ij2}) : 0 < \psi_{ij1} < \psi_{ij2} < T\}$ . The marginal prior distribution of  $\phi_{ij1}$  is uniform and the conditional prior distribution of  $\phi_{ij2}$  given  $\phi_{ij1}$  is also uniform. Similarly for  $\boldsymbol{\psi}_{ij}$  and  $\boldsymbol{\chi}_{ij}$ . Finally, the third prior consists of 2 truncated normal priors where, for each ENM  $i$  and response  $j$ , we define the following prior distributions for  $\boldsymbol{\phi}_{ij}$ ,  $\boldsymbol{\psi}_{ij}$ , and  $\boldsymbol{\chi}_{ij}$ .

$$\begin{aligned}\phi_{ij1} &\sim N(\phi_{o_{i1}}, \sigma_{\phi_{i1}}^2)I(0 < \phi_{ij1} < D), & \phi_{ij2} &\sim N(\phi_{o_{i2}}, \sigma_{\phi_{i2}}^2)I(\phi_{ij2} < \phi_{ij1} < D), \\ \psi_{ij1} &\sim N(\psi_{o_{i1}}, \sigma_{\psi_{i1}}^2)I(0 < \psi_{ij1} < T), & \psi_{ij2} &\sim N(\psi_{o_{i2}}, \sigma_{\psi_{i2}}^2)I(\psi_{ij2} < \psi_{ij1} < T), \\ \chi_{ij1} &\sim N(\frac{1}{3}DT, 100)I(0 < \chi_{ij1} < DT), & \chi_{ij2} &\sim N(\frac{2}{3}DT, 100)I(\chi_{ij2} < \chi_{ij1} < DT).\end{aligned}\tag{3}$$

For each ENM  $i$ , we also define the following prior distributions for our population level parameters:

$$\begin{aligned}\phi_{o_{i1}} &\sim N(\frac{1}{3}D, 10), & \phi_{o_{i1}} &\sim N(\frac{2}{3}D, 10), \\ \psi_{o_{i1}} &\sim N(\frac{1}{3}T, 10), & \psi_{o_{i1}} &\sim N(\frac{2}{3}T, 10).\end{aligned}\tag{4}$$

Finally, we specify priors on our hyperparameters as follows:

$$\begin{aligned} 1/\sigma_{\phi_{i1}}^2 &\sim \text{Gamma}(a_{\phi_{i1}}, b_{\phi_{i1}}), & 1/\sigma_{\phi_{i2}}^2 &\sim \text{Gamma}(a_{\phi_{i2}}, b_{\phi_{i2}}) \\ 1/\sigma_{\psi_{i1}}^2 &\sim \text{Gamma}(a_{\psi_{i1}}, b_{\psi_{i1}}), & 1/\sigma_{\psi_{i2}}^2 &\sim \text{Gamma}(a_{\psi_{i2}}, b_{\psi_{i2}}). \end{aligned} \quad (5)$$

For all other parameters we used relatively diffuse priors, as described in Appendix B. Our inferences are based on 20,000 MCMC samples after discarding a conservative 60,000 iterations for burn-in.

Figures 6 through 9 provide results from our simulation study using the three different prior models for our change-point parameters. Simulated dose (*column 2*), duration (*column 3*), and dose-time interaction (*column 4*) response curves are superimposed with expected dose and duration response curves and point-wise 95% posterior intervals estimated from our model. Finally, *column 1* shows fitted dose-response surfaces, spanning dose and time, for prior 2.

These figures show that the model is not very sensitive to our choice of prior parameters. Priors 1-3 are, in most cases, indistinguishable. The benefit of using the bivariate beta prior described in the paper is that it reflects the biological mechanism of toxicity. More specifically, it assigns zero probability to zero dose and time where toxicity is not expected to occur. The bivariate beta prior also takes a conservative standpoint by assigning high probability to low doses and times above a certain threshold, which biologically can be defined by the dosimetry of the particle.

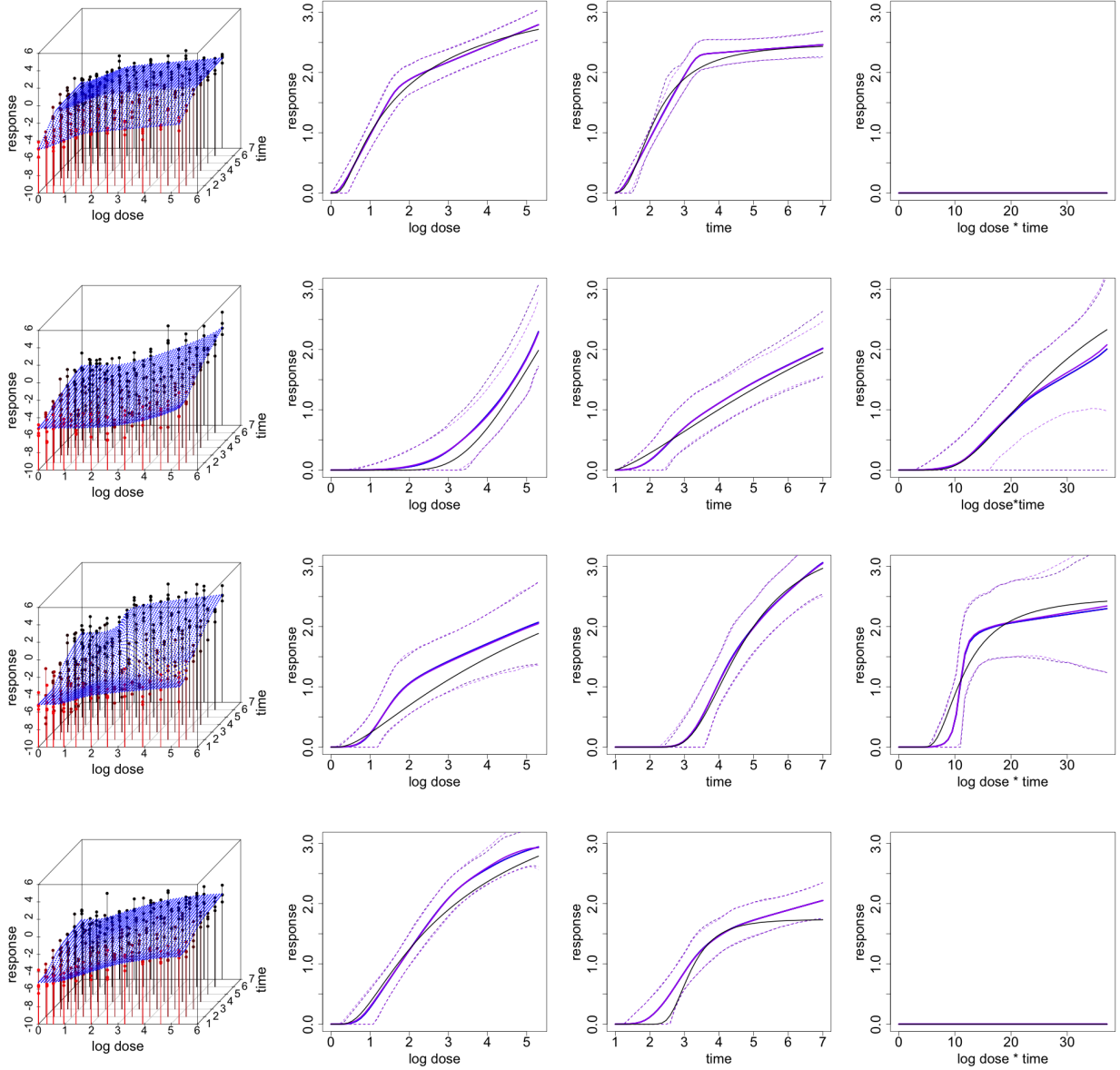


**Figure 6: Simulation study to assess sensitivity of prior model on the change-point parameters.** Simulated dose (*column 2*), duration (*column 3*), and dose-time interaction (*column 4*) response curves (black) superimposed with expected curves estimated from our model (solid colored lines) and point-wise 95% posterior intervals (dashed lines). Prior 1 (blue) is the bivariate beta prior presented in the paper, prior 2 (red) is a uniform prior over the simplex and prior 3 (purple) is the truncated normal prior described above. (*left*) Fitted response surfaces estimated using prior 2, superimposed with simulated data.

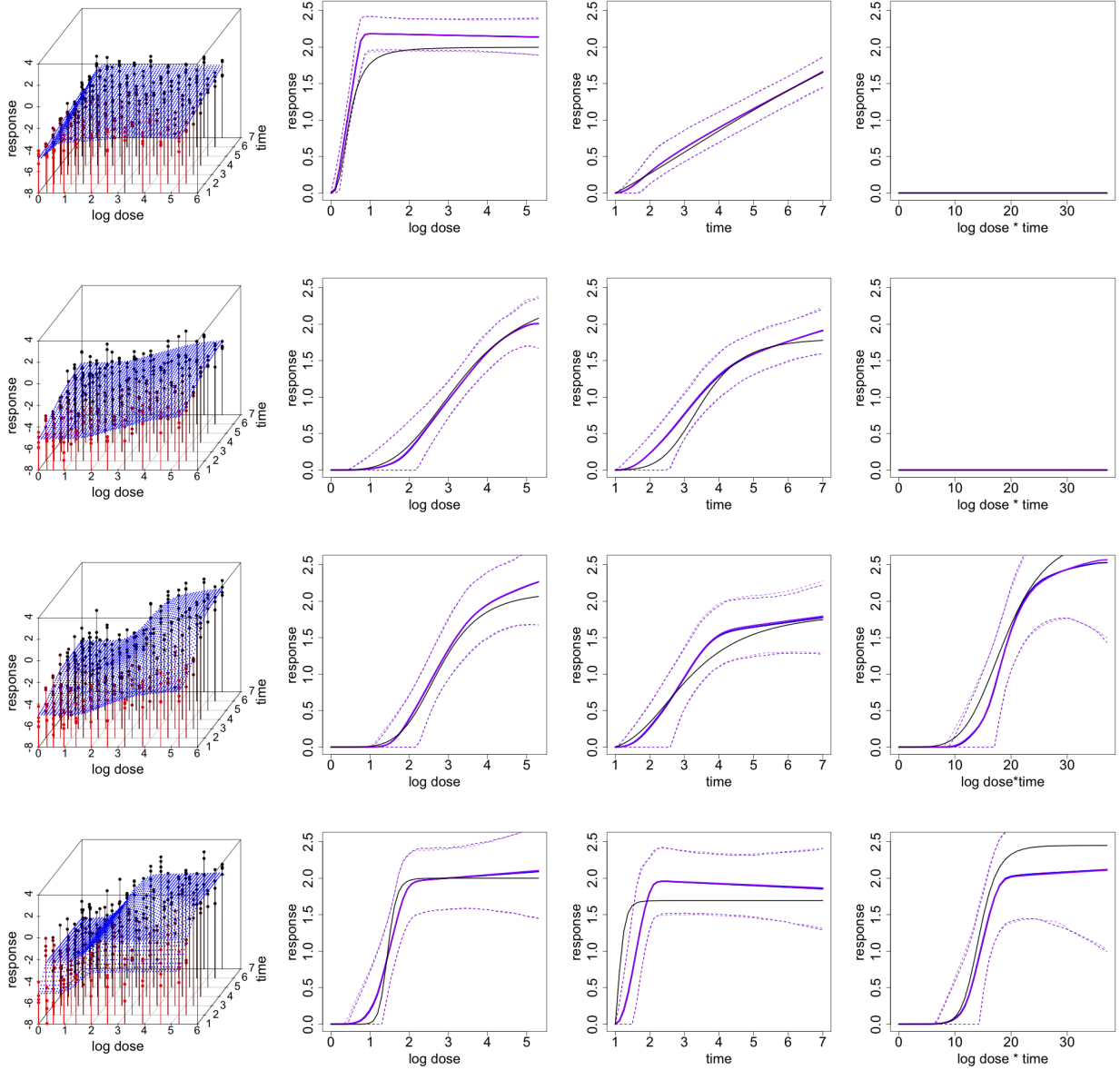


**Figure 7: Simulation study to assess sensitivity of prior model on the change-point parameters.** Simulated dose (*column 2*), duration (*column 3*), and dose-time interaction (*column 4*) response curves (black) superimposed with expected curves estimated from our model (solid colored lines) and point-wise 95% posterior intervals (dashed lines). Prior 1 (blue) is the bivariate beta prior presented in the paper, prior 2 (red) is a uniform prior over the simplex and prior 3 (purple) is the truncated normal prior described above. (*left*) Fitted response surfaces estimated using prior 2, superimposed with simulated data.

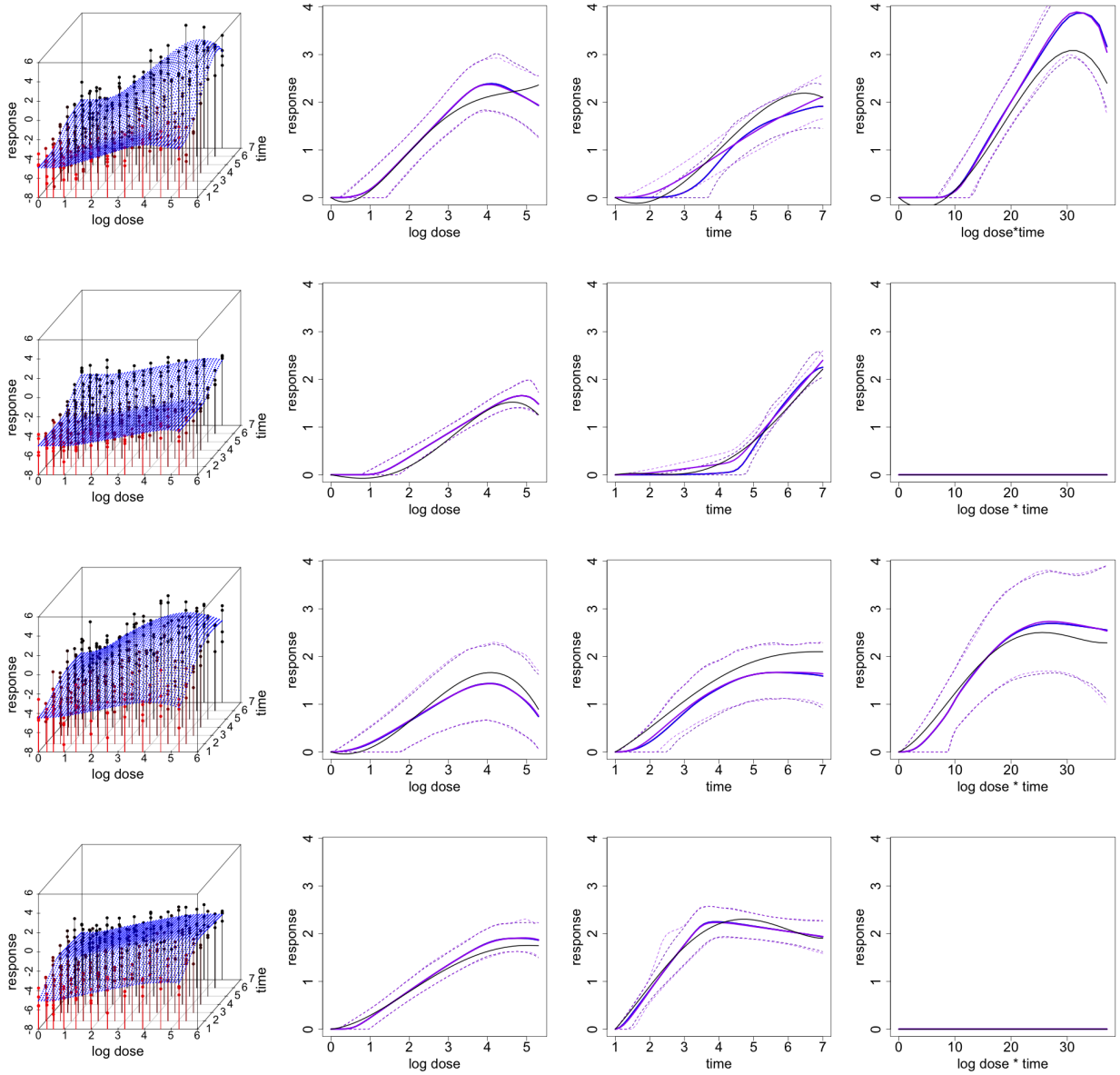


**Figure 8: Simulation study to assess sensitivity of prior model on the change-point parameters.** Simulated dose (*column 2*), duration (*column 3*), and dose-time interaction (*column 4*) response curves (black) superimposed with expected curves estimated from our model (solid colored lines) and point-wise 95% posterior intervals (dashed lines). Prior 1 (blue) is the bivariate beta prior presented in the paper, prior 2 (red) is a uniform prior over the simplex and prior 3 (purple) is the truncated normal prior described above. (*left*) Fitted response surfaces estimated using prior 2, superimposed with simulated data.

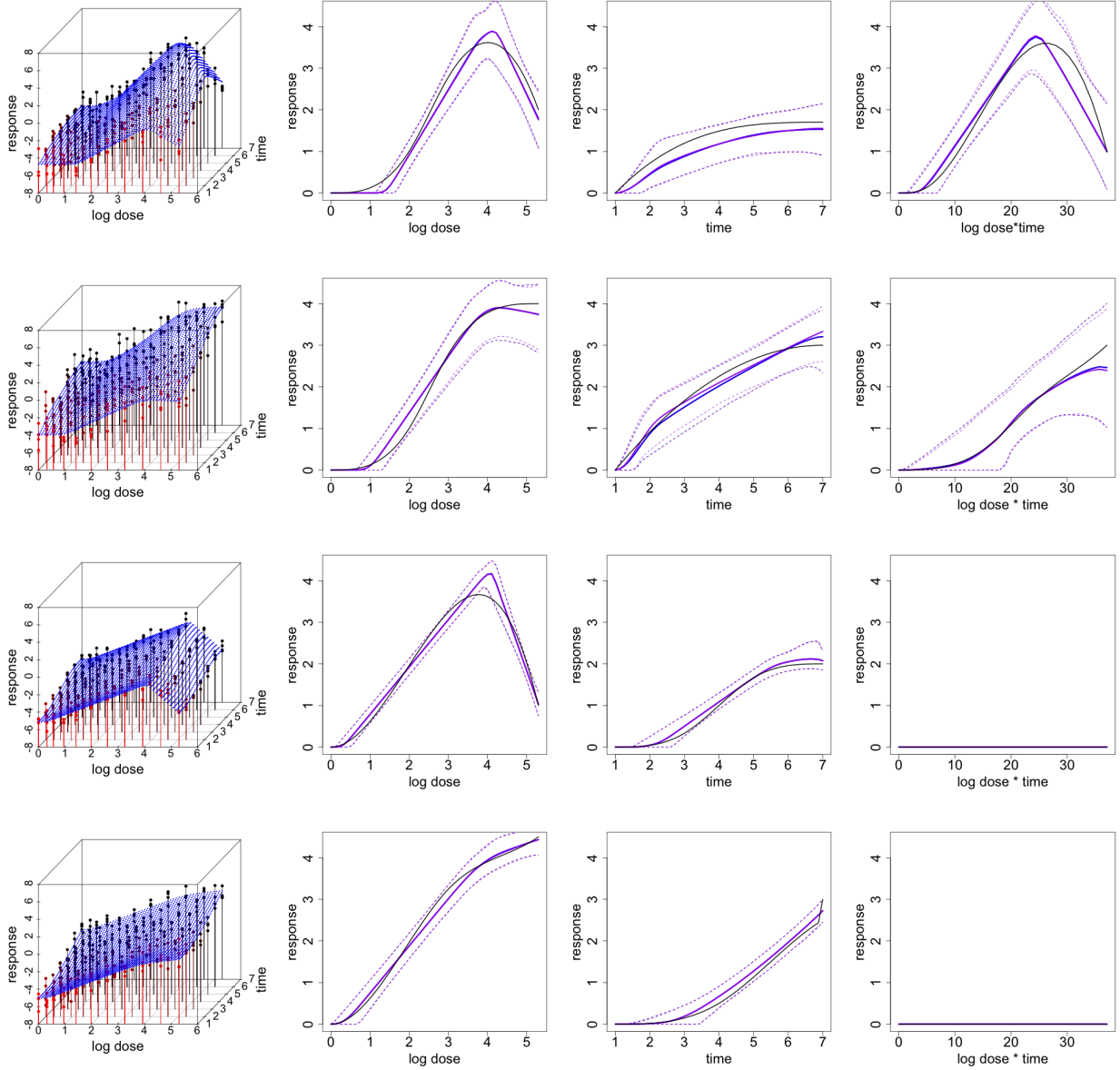


**Figure 9: Simulation study to assess sensitivity of prior model on the change-point parameters.** Simulated dose (*column 2*), duration (*column 3*), and dose-time interaction (*column 4*) response curves (black) superimposed with expected curves estimated from our model (solid colored lines) and point-wise 95% posterior intervals (dashed lines). Prior 1 (blue) is the bivariate beta prior presented in the paper, prior 2 (red) is a uniform prior over the simplex and prior 3 (purple) is the truncated normal prior described above. (*left*) Fitted response surfaces estimated using prior 2, superimposed with simulated data.

## APPENDIX D: FIGURES AND TABLES

The model presented in the paper was fit to data on eight metal and metal oxide nanoparticles, monitored in relation to four cytotoxicity parameters which, were measured over a grid of ten doses and seven times (hours) of exposure. The four responses include mitochondrial superoxide formation (MSF), loss of mitochondrial membrane potential (MMP), elevated intracellular calcium (EIC), and cellular membrane damage (CMD). Each outcome was measured as the percentage of cells positive for the response and was normalized using a logit transformation.

In this appendix we present figures for the remaining six particles not presented in the paper including, silver ( $Ag$ ), gold ( $Au$ ), aluminum oxide ( $Al_2O_3$ ), iron oxide ( $Fe_3O_4$ ), silicon dioxide ( $SiO_2$ ), and zinc oxide ( $ZnO$ ) (see Figures 10 to 15). Specifically, *column 1* shows fitted dose-response surfaces spanning dose and time. Also included are fitted curves for the expected dose response function  $f_{ij}(d)$  (*column 2*), which represent the effect due to dose, the expected duration response function  $g_{ij}(t)$  (*column 3*), which represent the effect due to time and, the expected dose-time interaction function  $h_{ij}(t)$  (*column 4*).

Figures 16 and 17 provides a plot of the estimated median response, relative to the background, for different doses and times of exposure. Blue colors indicate safety regions or areas of reduced risk to the cells, while red colored regions indicate increased risk of cytotoxicity. Finally, Table 2 provides posterior estimates of the expected inclusion probability of the dose-time interaction function. These probabilities can be used to test for a dose-time interaction, adjusted for multiplicity.

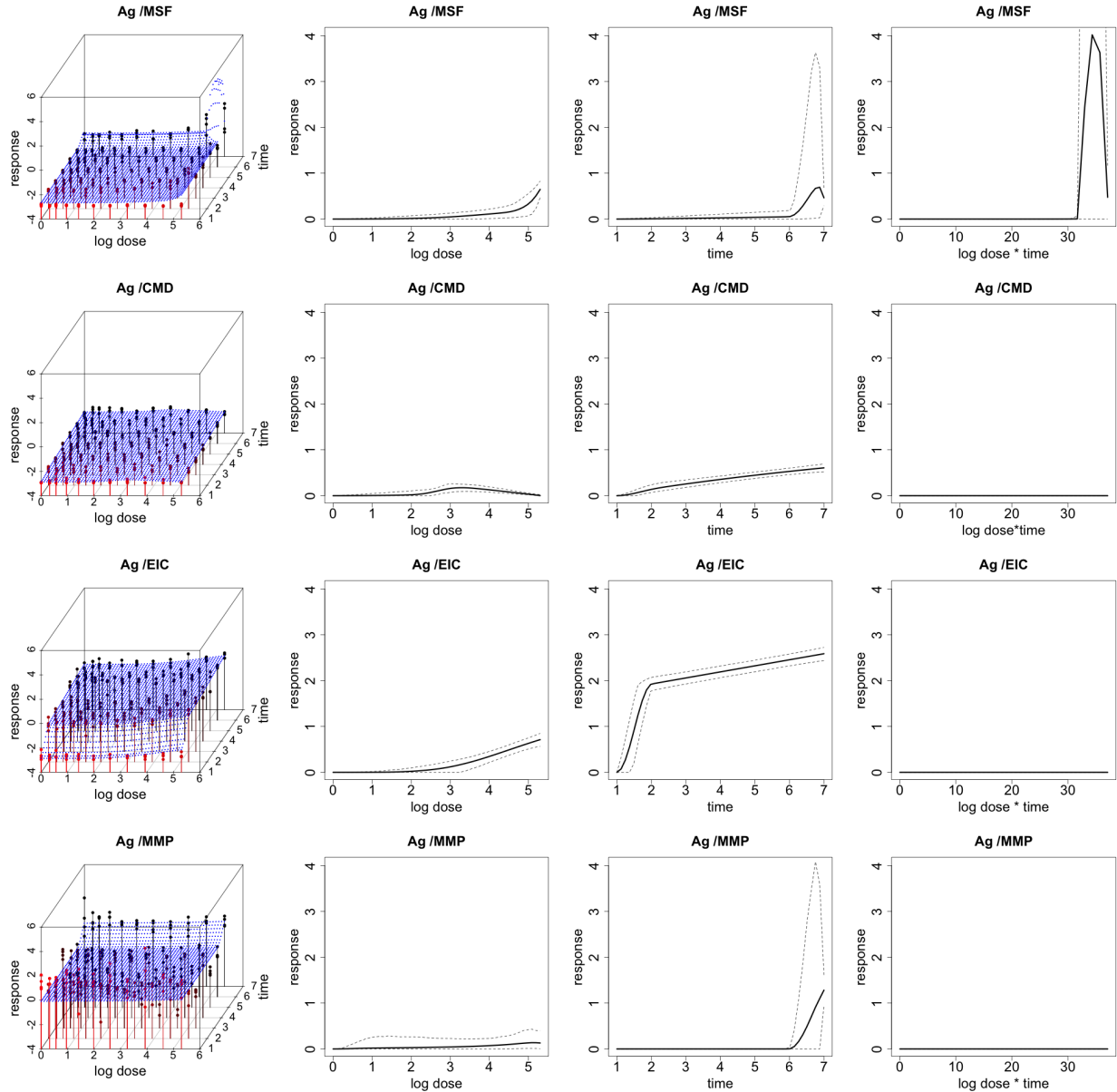


**Figure 10: Fitted response curves for the silver nanomaterial ( $Ag$ ).** Fitted response surfaces (column 1), dose-response function,  $f_{ij}(d)$  (column 2), duration-response function,  $g_{ij}(t)$  (column 3), dose/duration interaction function,  $h_{ij}(dt)$  (column 4) and associated 95% posterior intervals.

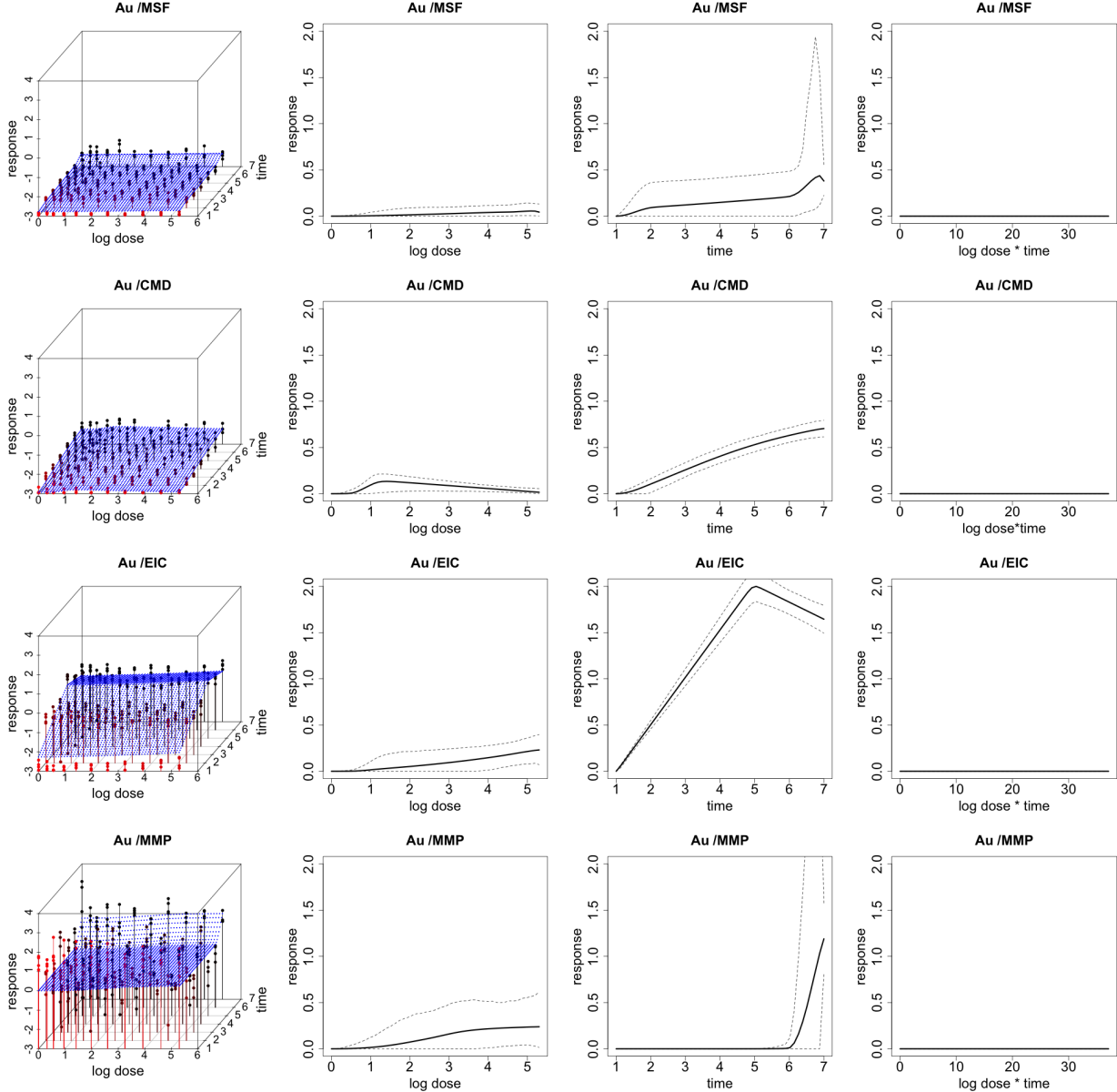


Figure 11: **Fitted response curves for the gold nanomaterial ( $Au$ ).** Fitted response surfaces (column 1), dose-response function,  $f_{ij}(d)$  (column 2), duration-response function,  $g_{ij}(t)$  (column 3), dose/duration interaction function,  $h_{ij}(dt)$  (column 4) and associated 95% posterior intervals.

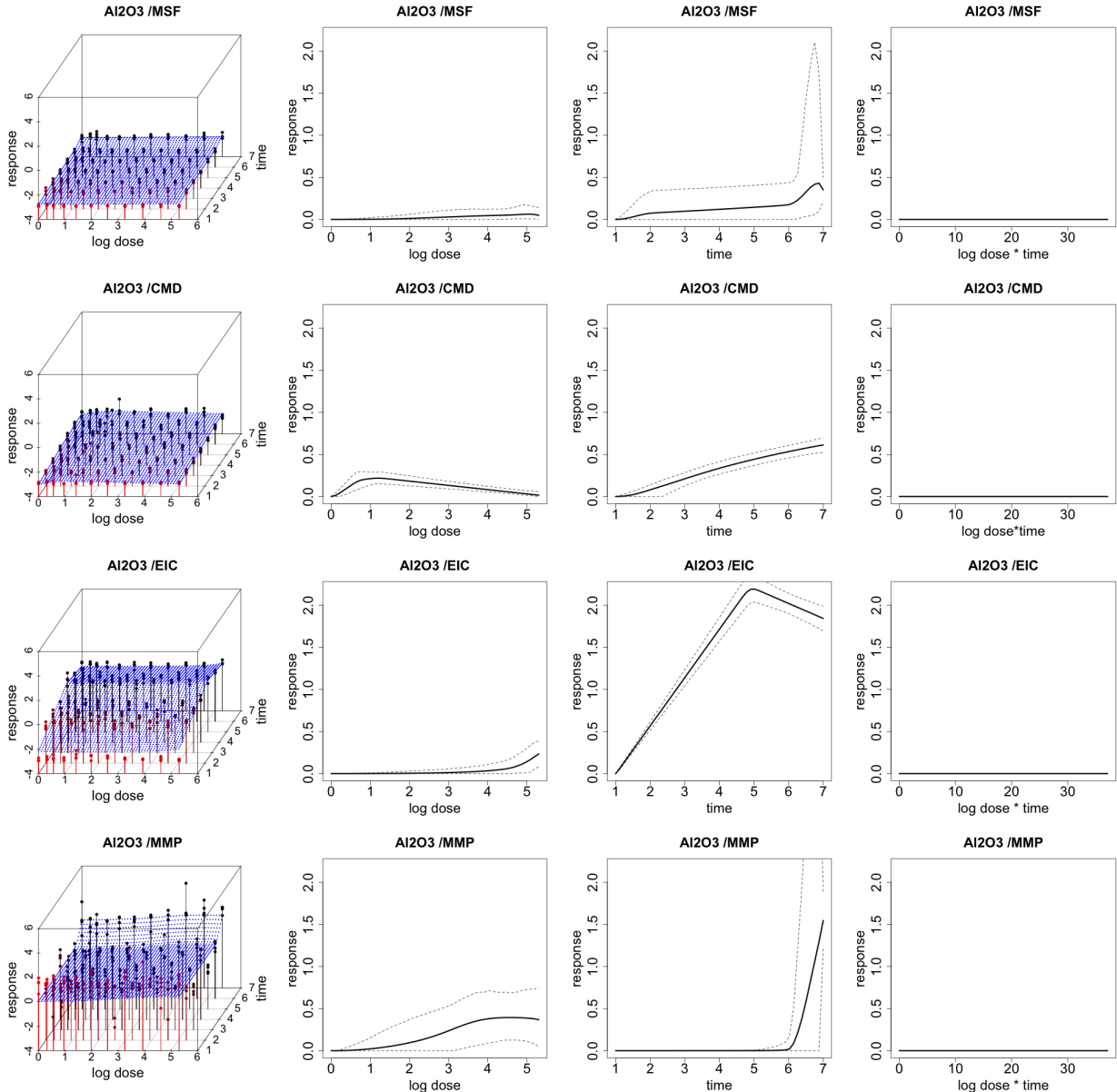


Figure 12: **Fitted response curves for the aluminum oxide nanomaterial ( $\text{Al}_2\text{O}_3$ ).** Fitted response surfaces (column 1), dose-response function,  $f_{ij}(d)$  (column 2), duration-response function,  $g_{ij}(t)$  (column 3), dose/duration interaction function,  $h_{ij}(dt)$  (column 4) and associated 95% posterior intervals.

ENM	MSF	EIC	CMD	MMP
<i>Ag</i>	0.59	0.00	0.00	0.99
<i>Au</i>	0.00	0.00	0.00	0.00
<i>Pt</i>	0.99	0.00	0.00	0.00
<i>Al<sub>2</sub>O<sub>3</sub></i>	0.00	0.00	0.00	0.00
<i>Fe<sub>3</sub>O<sub>4</sub></i>	0.99	0.00	0.00	0.00
<i>SiO<sub>2</sub></i>	0.99	0.00	0.00	0.46
<i>QD</i>	0.99	0.00	0.00	0.00
<i>ZnO</i>	0.99	0.00	0.99	0.00

Table 2: **Expected inclusion probability of the dose-time interaction function.** Posterior mean estimates of  $\rho_{ij}$  for each particle and outcome. Expected inclusion probabilities can be used to test for a dose-time interaction.

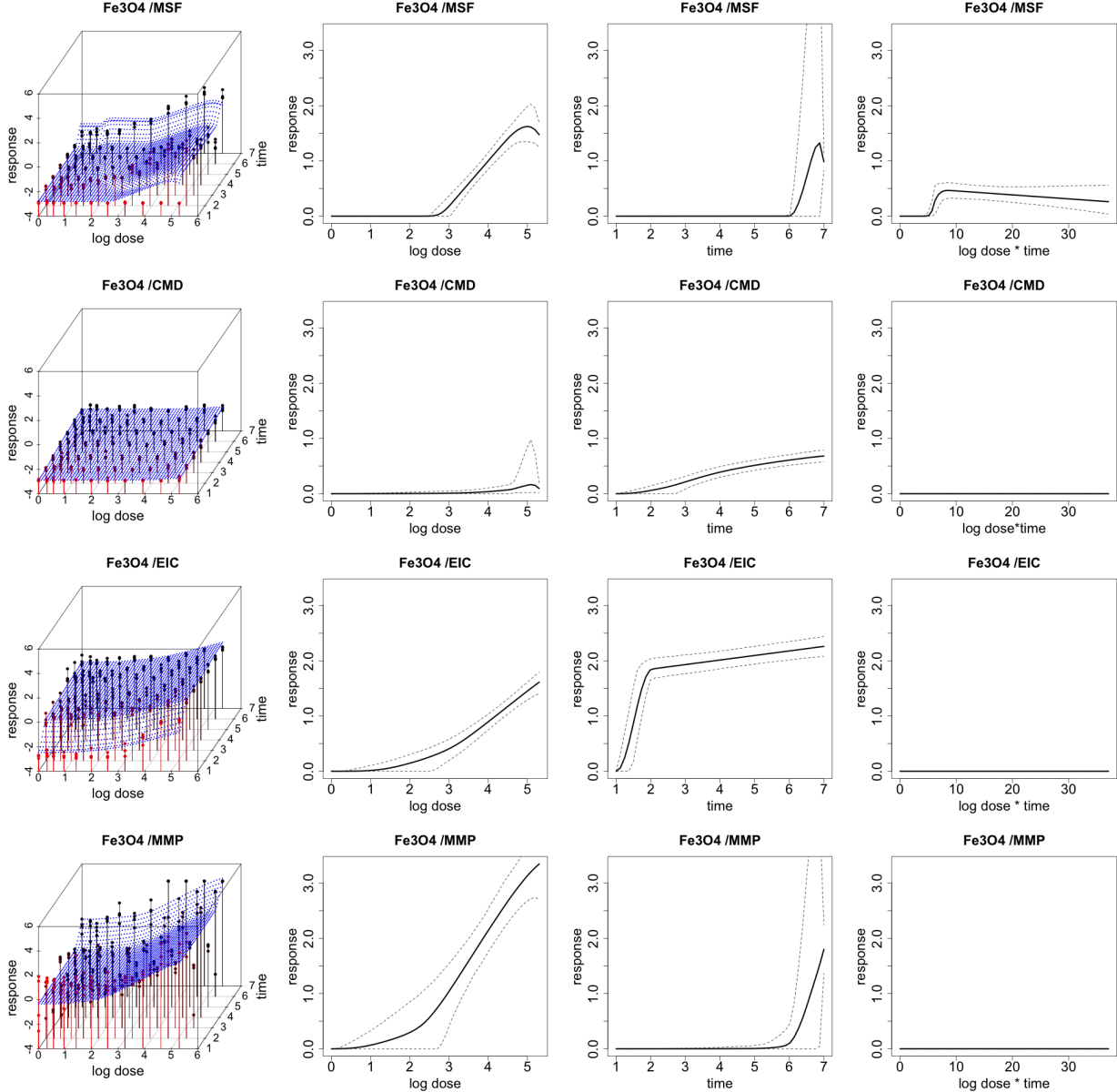


Figure 13: **Fitted response curves for the iron oxide nanomaterial ( $Fe_3O_4$ )**. Fitted response surfaces (column 1), dose-response function,  $f_{ij}(d)$  (column 2), duration-response function,  $g_{ij}(t)$  (column 3), dose/duration interaction function,  $h_{ij}(dt)$  (column 4) and associated 95% posterior intervals.

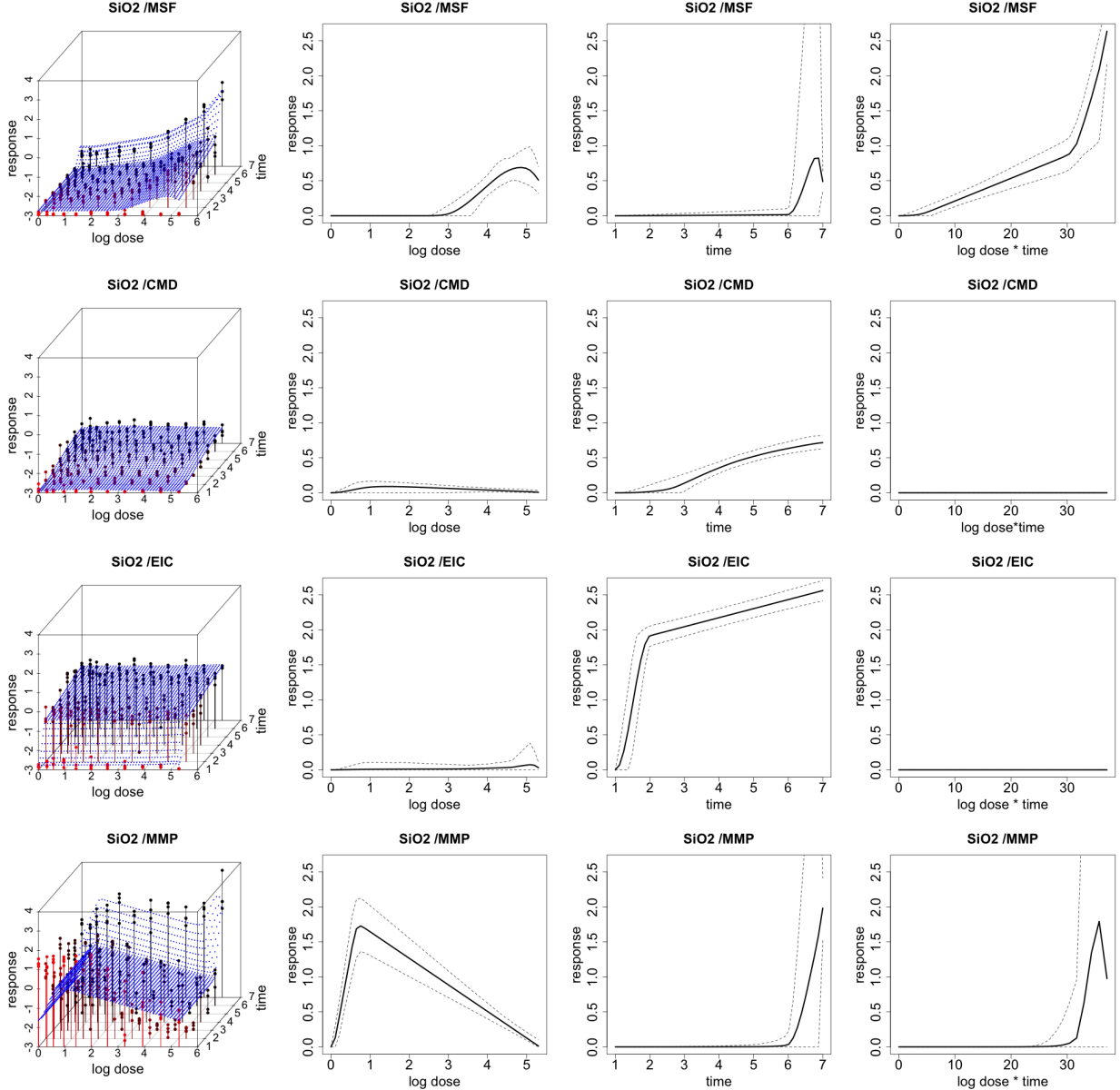


Figure 14: **Fitted response curves for the silicon dioxide nanomaterial ( $SiO_2$ ).** Fitted response surfaces (column 1), dose-response function,  $f_{ij}(d)$  (column 2), duration-response function,  $g_{ij}(t)$  (column 3), dose/duration interaction function,  $h_{ij}(dt)$  (column 4) and associated 95% posterior intervals.

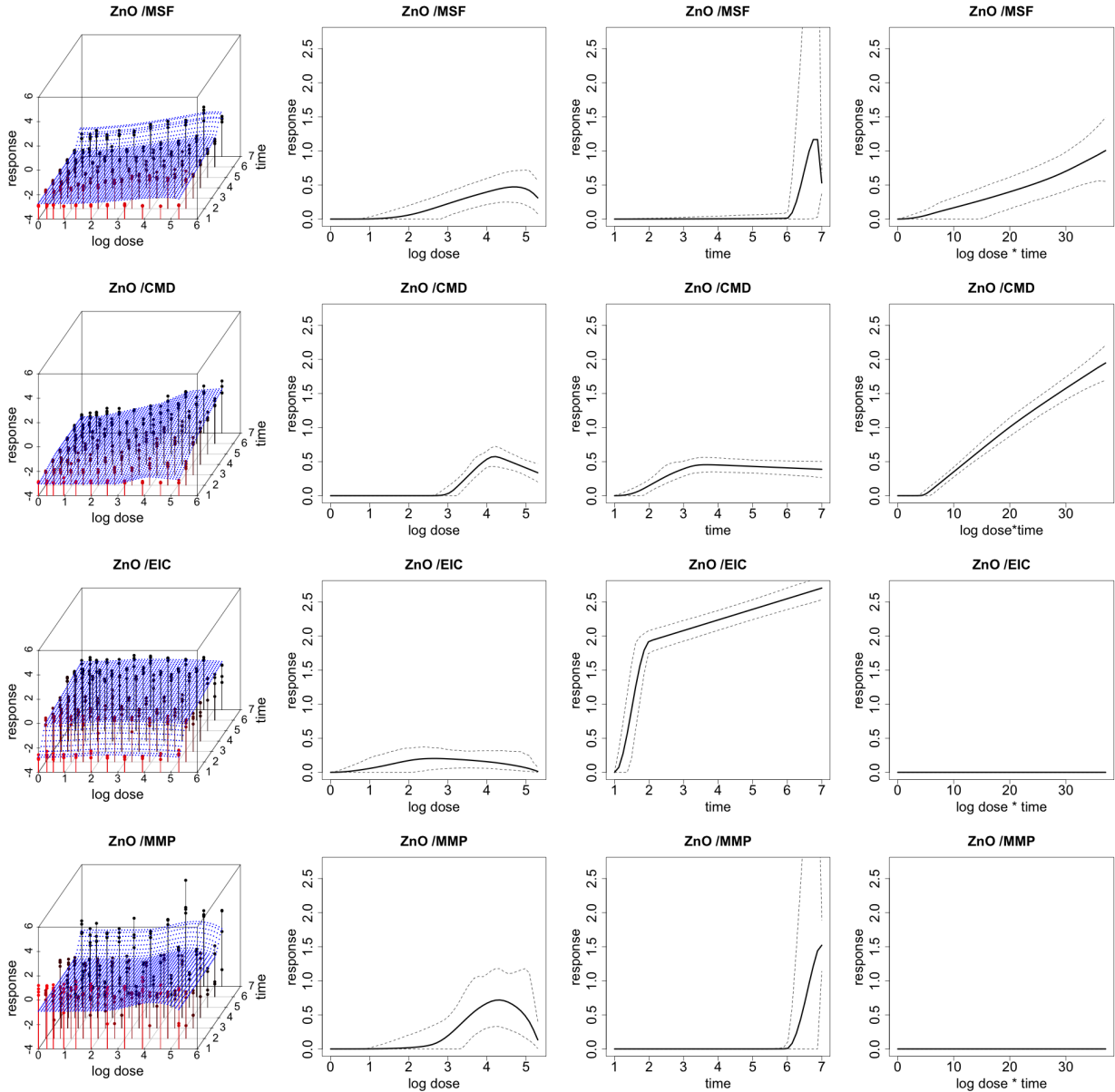
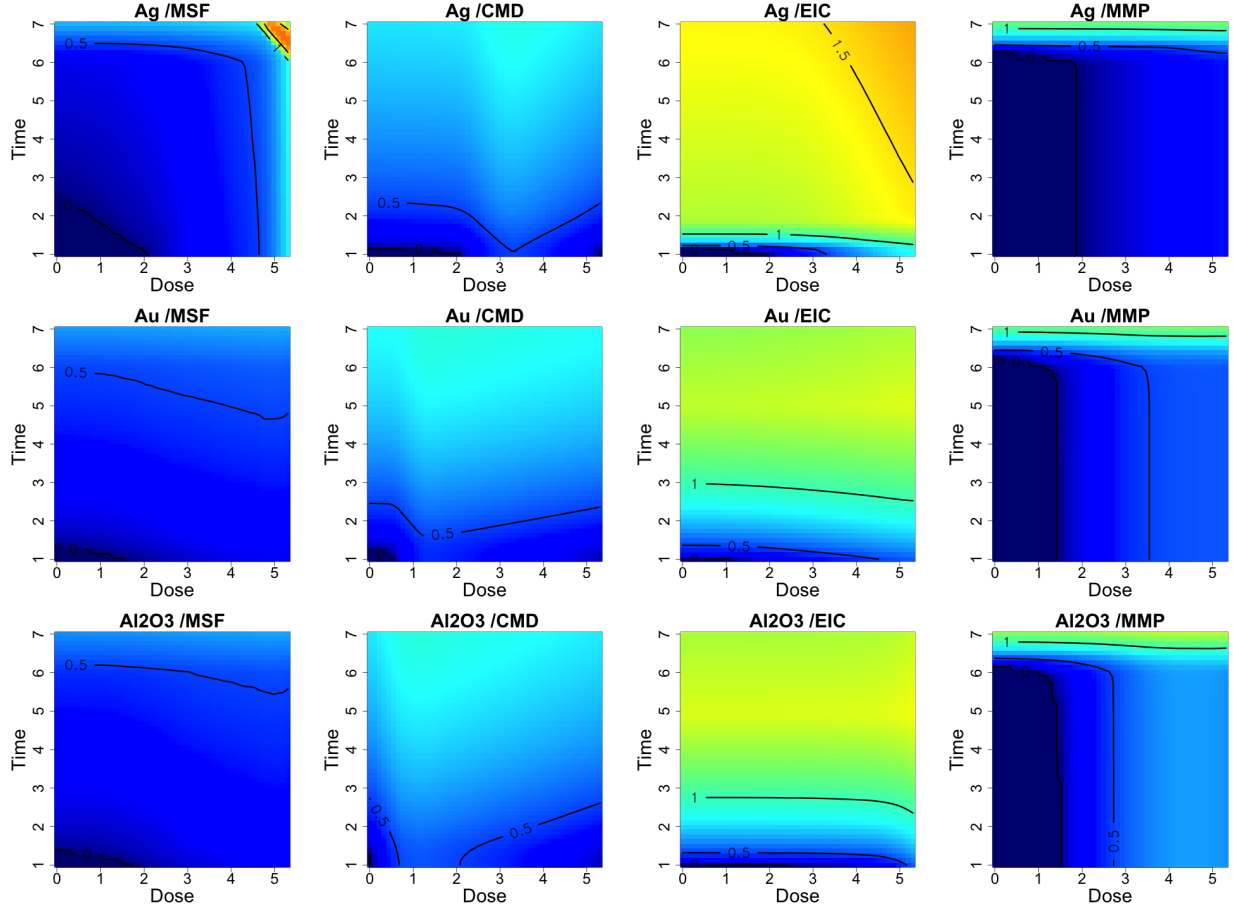
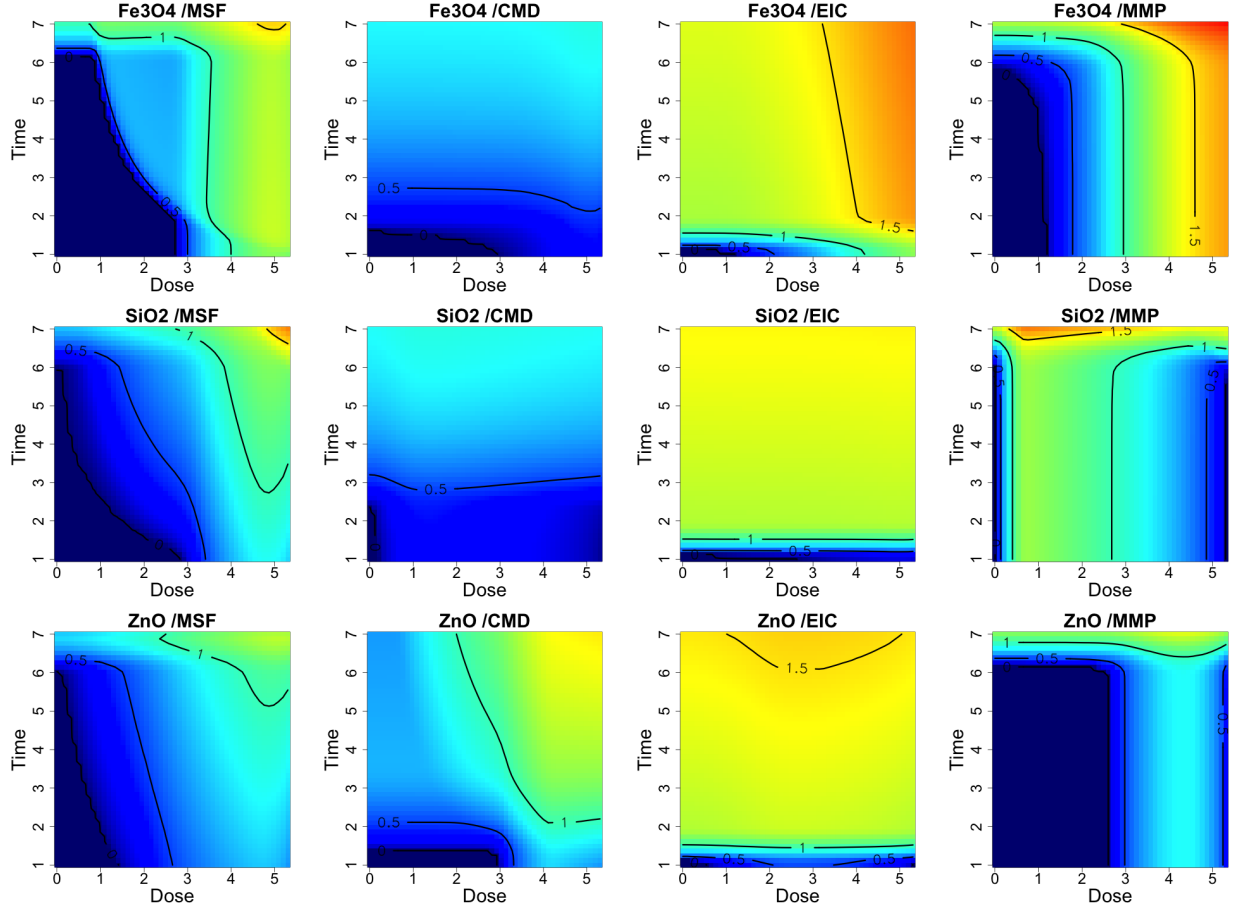


Figure 15: **Fitted response curves for the quantum dot nanomaterial ( $ZnO$ ).** Fitted response surfaces (column 1), dose-response function,  $f_{ij}(d)$  (column 2), duration-response function,  $g_{ij}(t)$  (column 3), dose/duration interaction function,  $h_{ij}(dt)$  (column 4) and associated 95% posterior intervals.



**Figure 16: Safe exposure regions.** For each particle and outcome we can define dose and time exposure regions which do not induce cytotoxicity. Lighter regions indicate greater cytotoxicity to the cells, whereas darker regions indicate reduced risk. Contour lines quantitate the median estimated response, relative to the background, where zero response areas can be interpreted as safe exposure regions.



**Figure 17: Safe exposure regions.** For each particle and outcome we can define dose and time exposure regions which do not induce cytotoxicity. Red colored regions indicate greater cytotoxicity to the cells, whereas blue colored regions indicate reduced risk. Contour lines quantitate the median estimated response, relative to the background, where zero response areas can be interpreted as safe exposure regions.